Supporting Information

A binuclear Co-based metal-organic framework towards efficient oxygen evolution reaction

Ning Liu, Qiaoqiao Zhang, and Jingqi Guan*

Institute of Physical Chemistry, College of Chemistry, Jilin University, Changchun 130012, PR China.

*E-mail: guanjq@jlu.edu.cn (J. Guan)

Materials

All chemicals were analytical grade and were used as purchased without further purification. Solutions were prepared using high purity water (Millipore Milli-Q purification system, resistivity > 18 MΩ·cm).

Synthesis of Co_2-tzpa

291 mg $Co(NO_3)_2 \cdot 6H_2O$ and 155 mg H_3tzpa were dissolved in a mixture of H_2O (3 mL) and DMF (4 mL), which was transferred into 20 mL Teflon autoclave and heated at 105 °C for 72 h. After filtrated, washed with deionized water and dried at 60 °C overnight, the red block crystals were obtained, which is nominated as Co_2-tzpa.

Material characterizations

Scanning electron microscope (SEM) images were observed by a Hitachi SU8020. The valence state of metal was determined using XPS recorded on a Thermo ESCALAB 250Xi. The X-ray source selected was monochromatized Al Kα source (15 kV, 10.8 mA). Region scans were collected using a 20 eV pass energy.

Electrochemical activity characterizations

All electrochemical measurements were performed in a three-electrode system with a glassy carbon electrode (GCE) as the substrate for the working electrode, a graphite rod as the counter electrode and a saturated calomel electrode as the reference electrode. The reference electrode was calibrated with respect to a reversible hydrogen electrode before each experiment. The glassy carbon electrode was pre-polished using 0.05 μm alumina and distilled water. To prepare the working electrode, 2 mg of the catalyst was dispersed in a 0.5 mL mixed solvent of ethanol and Nafion (0.25 wt%) and sonicated to obtain a homogeneous ink. 5 μL of the catalyst ink was drop-casted on the glassy carbon electrode and dried at room temperature (catalyst loading: 0.28 $mg \cdot cm^{-2}$).

For OER, the working electrode was first activated by steady-state cyclic voltammetry (CV) performed in the potential range from 1.0 to 1.6 V vs RHE at a scan rate of 50 mV s^{-1} for 50 cycles. Linear scan voltammetry (LSV) curves were then collected at a scan rate of 5 mV s^{-1}. All of the potentials in the LSV polarization curves

were with 90% *i*R compensation unless specifically illustrated.

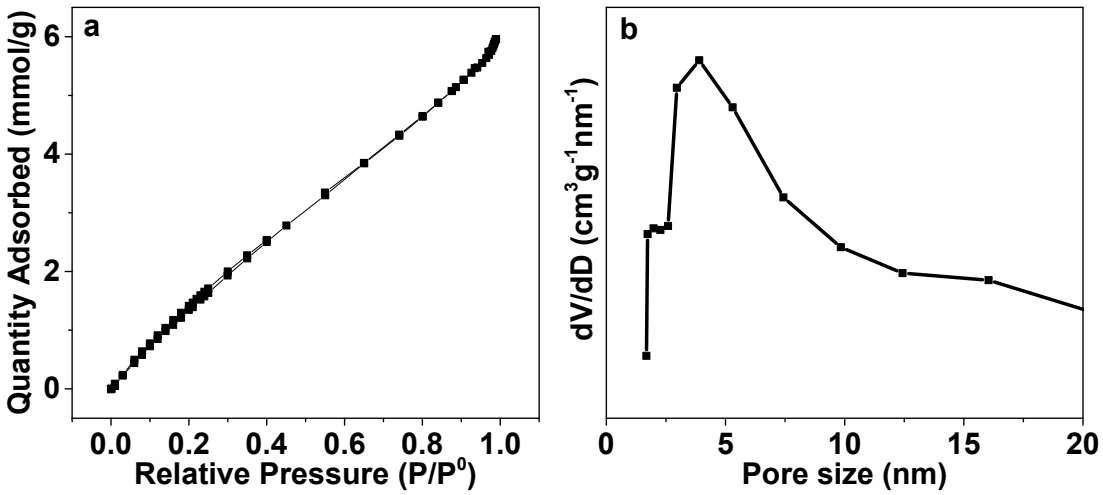

Figure S1. (a) N_2 adsorption−desorption isotherms and (b) pore size distribution of Co_2-tzpa.

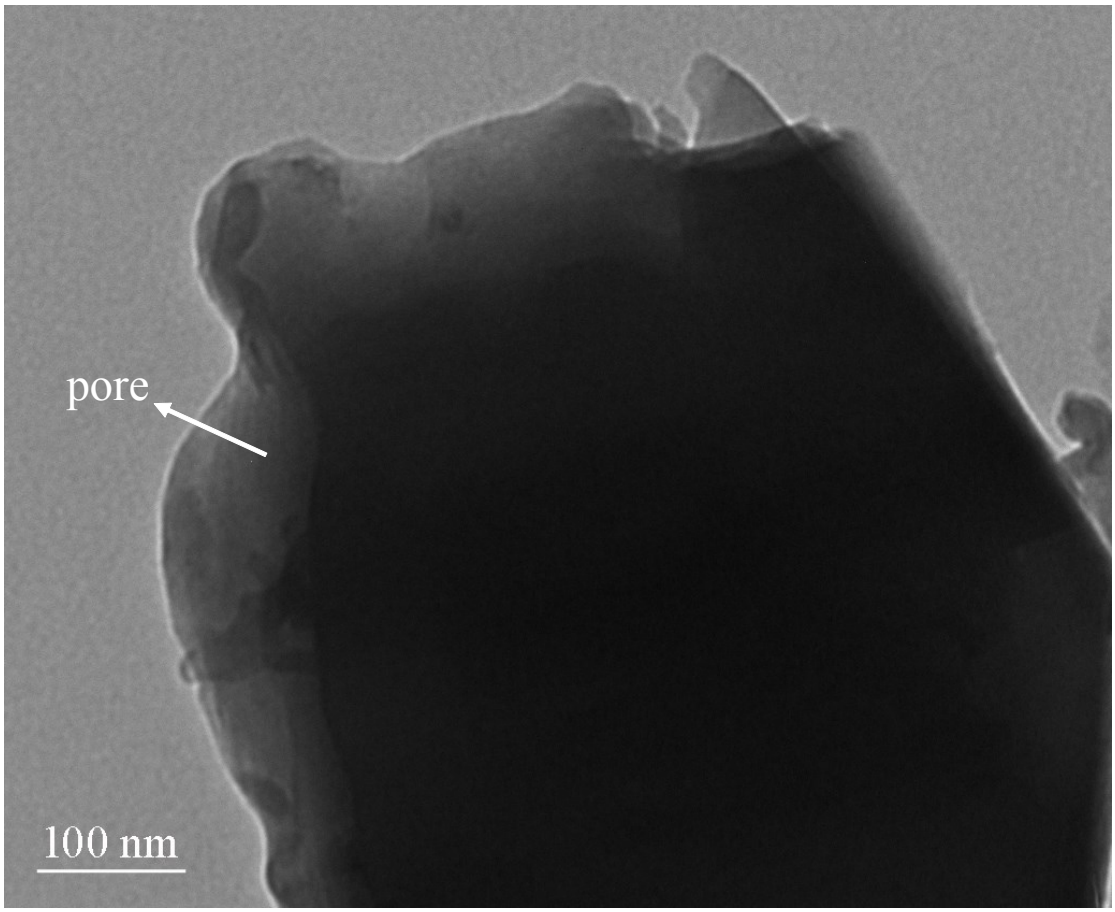

Figure S2. TEM image of Co_2-tzpa.

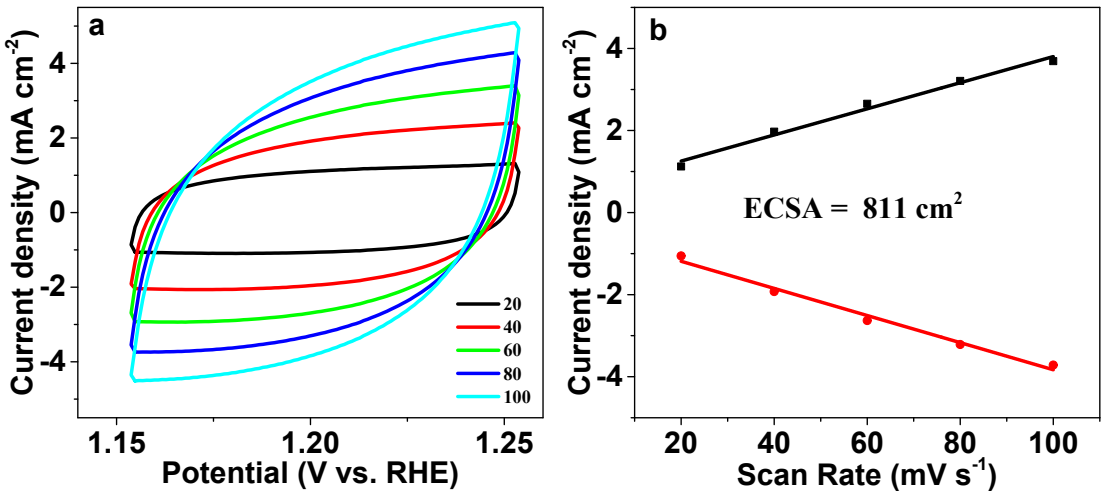

Figure S3. (a) CVs measured in a non-Faradaic region at scan rate of 10 mV s^{-1}, 20 mV s^{-1}, 40 mV s^{-1}, 60 mV s^{-1}, 80 mV s^{-1}, and 100 mV s^{-1} for Co_2-tzpa. (b) The cathodic (black) and anodic (red) currents measured at 1.203 V vs RHE as a function of the scan rate. The average of the absolute value of the slope is taken as the double-layer capacitance of the electrode.

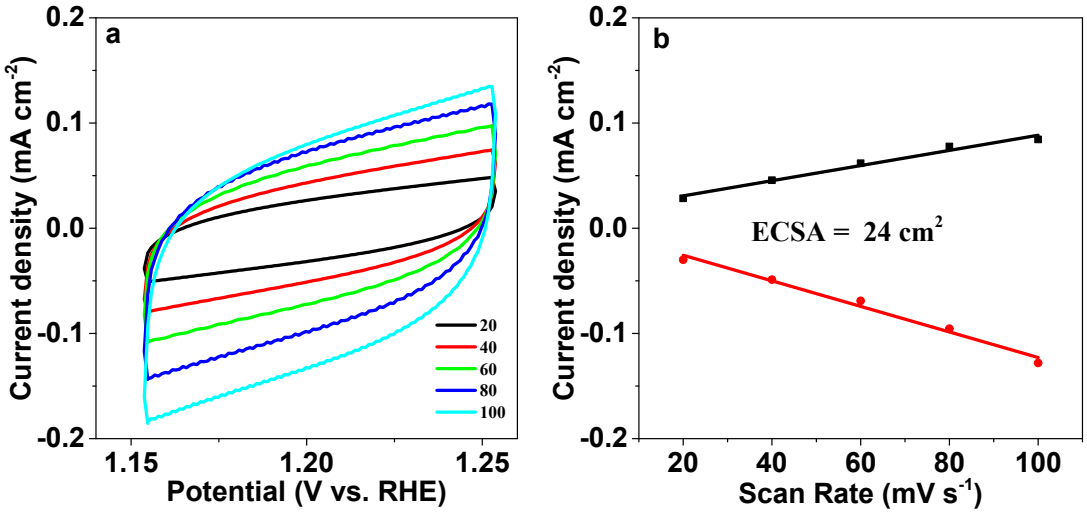

Figure S4. (a) CVs measured in a non-Faradaic region at scan rate of 10 mV s^{-1}, 20 mV s^{-1}, 40 mV s^{-1}, 60 mV s^{-1}, 80 mV s^{-1}, and 100 mV s^{-1} for nano-Co_3O_4. (b) The cathodic (black) and anodic (red) currents measured at 1.203 V vs RHE as a function of the scan rate. The average of the absolute value of the slope is taken as the double-layer capacitance of the electrode.

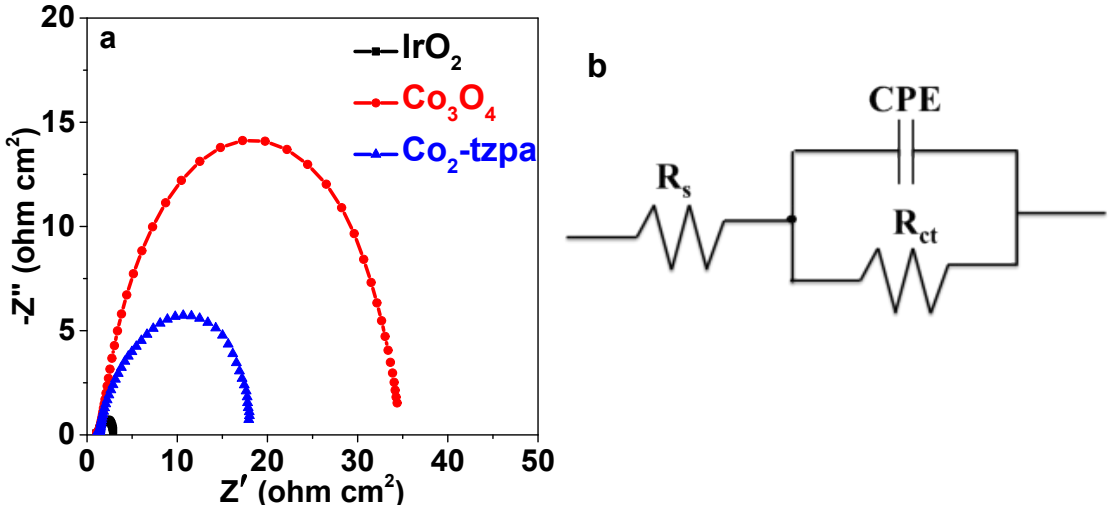

Figure S5. (a) Nyquist plots of the EIS test for commercial IrO_2, nano-Co_3O_4, and Co_2-tzpa. (b) The equivalent circuit used for fitting the Nyquist plots. Rs represents the uncompensated electrolyte resistance, CPE represents the constant phase element, and R_{ct} represents the resistance of charge transfer.

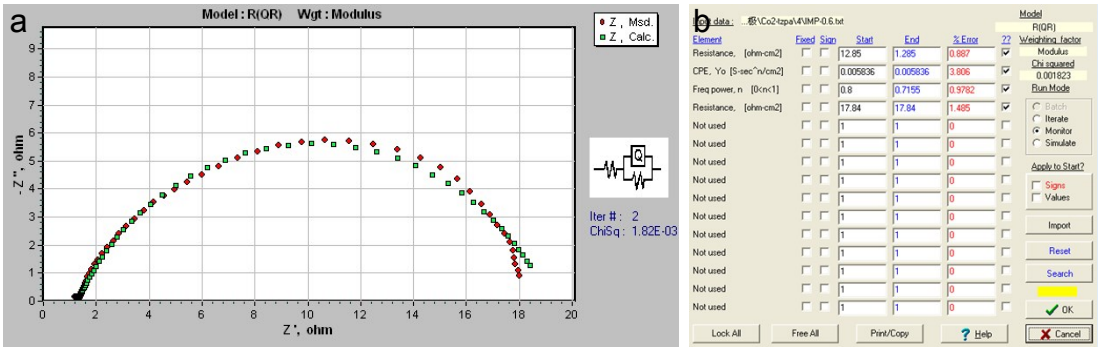

Figure S6. (a) Fitted EIS spectrum and (b) the specific fitting data for Co_2-tzpa.

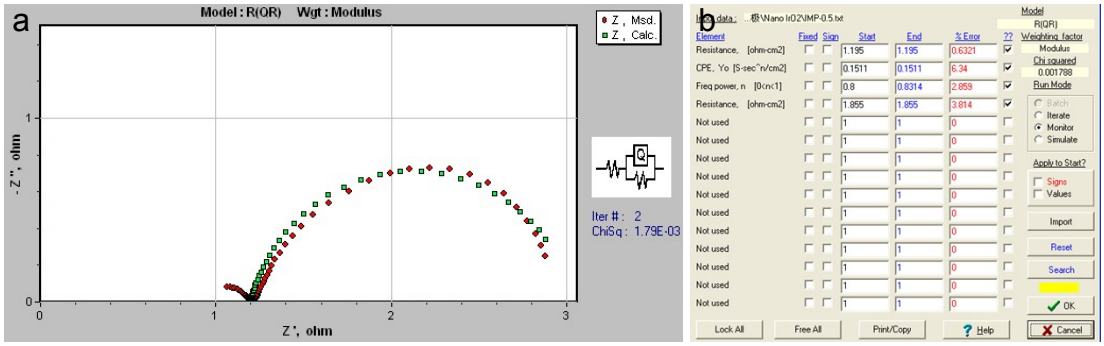

Figure S7. (a) Fitted EIS spectrum and (b) the specific fitting data for IrO_2.

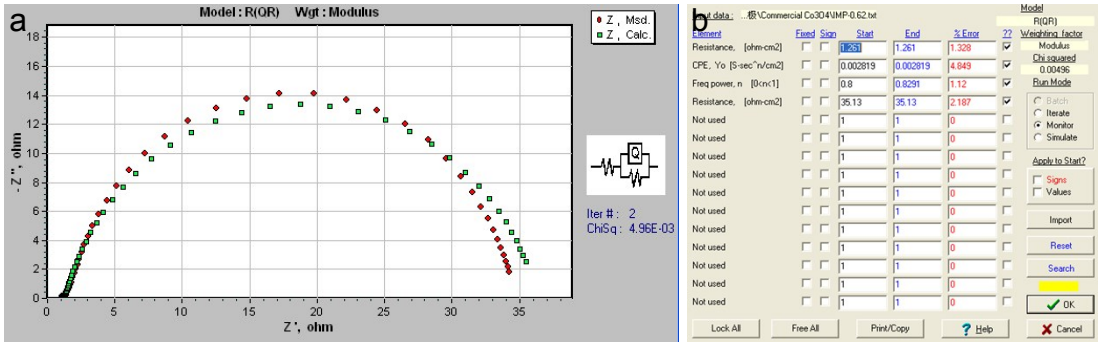

Figure S8. (a) Fitted EIS spectrum and (b) the specific fitting data for nano-Co_3O_4.

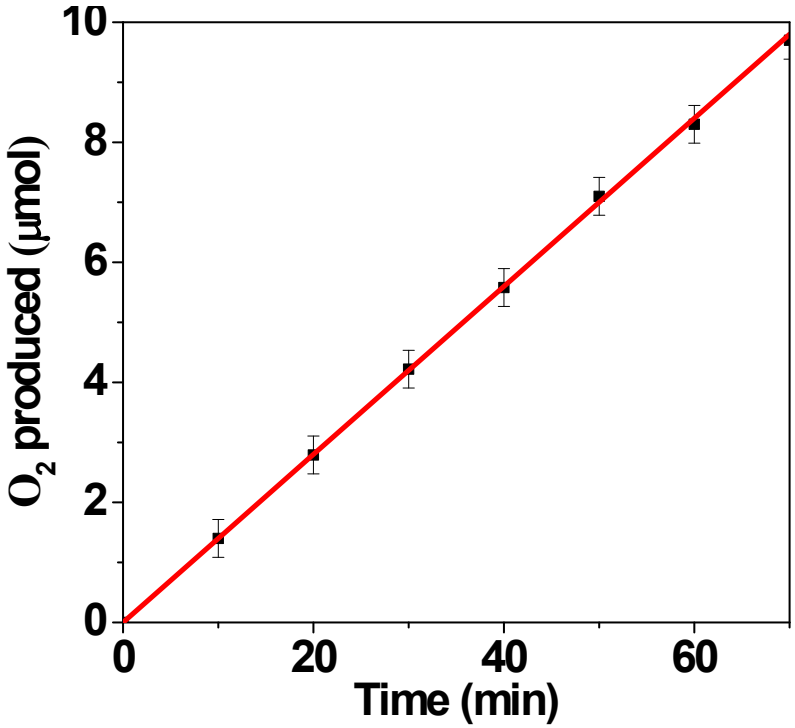

Figure S9. The molar number of O_2 produced as a function of time. The straight line represents the theoretically calculated amounts of O_2 assuming 100% Faradaic efficiency, and the scattered blocks represent the produced O_2 measured by gas chromatography. The overlapping of these two sets of data indicates that nearly all the current is due to O_2 evolution.

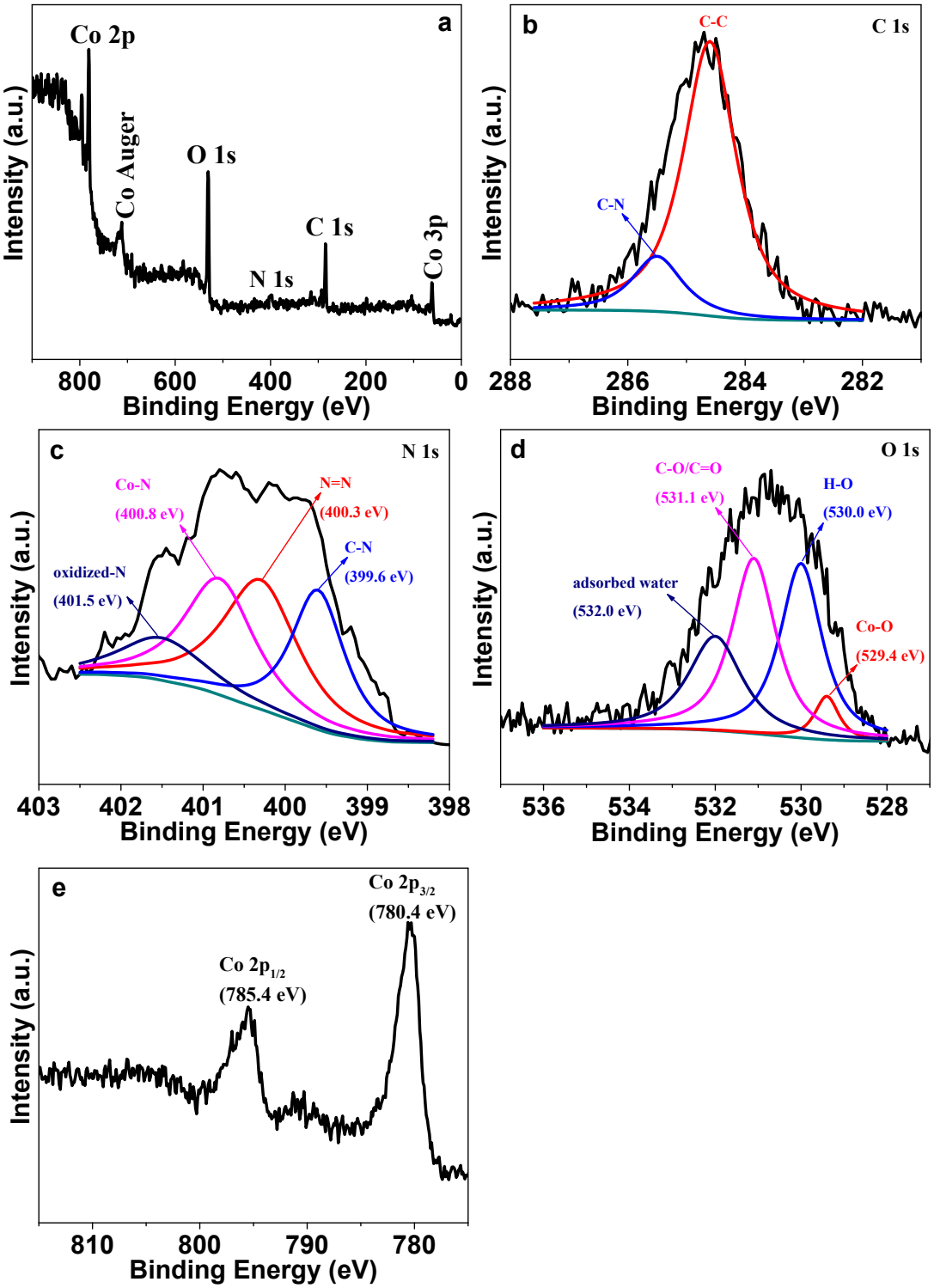

Figure S10. (a) XPS survey spectrum. (b-e) high resolution XPS spectra of the used Co_2-tzpa catalyst after OER stability test.

Table S1. Comparison of OER performance of Co_2-tzpa with results in recent literature

MOF	Catalyst	Electrolyte	Overpotential (mV) at 10 mA cm^{-2}	Ref.
Co_2-tzpa	Co_2-tzpa	1 M KOH	336	This work
Co_2-tzpa	Co_2-tzpa	0.1 M KOH	396	This work
Co_xFe_y NH_2-MIL-88B	$Co_{0.17}Fe_{0.79}P$/NC	1 M KOH	299	[1]
Co-MOF-74	$LaCoO_{3-\delta}$	0.1 M KOH	330	[2]
Co-MOF-74	BC/Co_3O_4	1 M KOH	310	[3]
Co-MOF-74	$Fe(OH)_3$@Co-MOF-74	1 M KOH	292	[4]
Ni-MOF-74	Fe_2O_3@Ni-MOF-74	1 M KOH	264	[5]
NiMOF-74	NGO/Ni_7S_6	0.1 M KOH	380	[6]
NiO–MOF-74	Porous Ni_2P nanosheets	1 M KOH	320	[7]
Co-(III)$_2$(HCOO)$_2$(BPTC)	BMM-11	1 M KOH	362	[8]
$[Co(L1)(HL3)_2\cdot(H_2O)_2]_n$	$[Co(L1)(HL3)_2\cdot(H_2O)_2]_n$	1 M KOH	398	[9]
Co_2(benzimidazole)$_4$	M-PCBN/CC	1 M KOH	348	[10]
Co_3-btca	$Co_{2.36}Fe_{0.19}Ni_{0.45}$-btca	1 M KOH	292	[11]
$Co_3(\mu_3\text{-OH})(COO)_6$	Co@NPC	1 M NaOH	540	[12]
$Co_3[Co(CN)_6]_2$	PB-Co/Co−NPHCS	0.1 M KOH	370	[13]
$[Co_4(OH)_2]^{6+}$	TMOF-4 nanosheets	1 M KOH	318	[14]
UTSA-16	UTSA-16	1 M KOH	408	[15]
Co_4(2-min)$_6WO_4\cdot$1.5DMF	Co/W-C@NCNSs	1 M KOH	323	[16]
CTGU-14	SnO_2 & CTGU-14	0.1 M KOH	388	[17]
$Co_2(OH)_2$DBC	Co-MONs	1 M KOH	309	[18]
Co-BTC	$CoSe_2$	1 M KOH	330	[19]
Co-BTC	Co2P@C	1 M KOH	328	[20]

References

1. J. Chen, Y. Zhang, H. Ye, J.-Q. Xie, Y. Li, C. Yan, R. Sun and C.-P. Wong, *ACS Appl. Energy Mater.*, 2019, **2**, 2734-2742.
2. X. Wang, L. Ge, Q. Lu, J. Dai, D. Guan, R. Ran, S.-C. Weng, Z. Hu, W. Zhou and Z. Shao, *J. Power Sources*, 2020, **468**, 228377.
3. L. Zou and Q. Xu, *Chem Asian J*, 2020, **15**, 490-493.
4. Z. Gao, Z. W. Yu, F. Q. Liu, C. Yang, Y. H. Yuan, Y. Yu and F. Luo, *ChemSusChem*, 2019, **12**, 4623-4628.
5. Z. Gao, Z. W. Yu, F. Q. Liu, Y. Yu, X. M. Su, L. Wang, Z. Z. Xu, Y. L. Yang, G. R. Wu, X. F. Feng and F. Luo, *Inorg. Chem.*, 2019, **58**, 11500-11507.
6. K. Jayaramulu, J. Masa, O. Tomanec, D. Peeters, V. Ranc, A. Schneemann, R. Zboril, W. Schuhmann and R. A. Fischer, *Adv. Funct. Mater.*, 2017, **27**, 1700451.
7. Q. Wang, Z. Liu, H. Zhao, H. Huang, H. Jiao and Y. Du, *J. Mater. Chem. A*, 2018, **6**, 18720-18727.
8. L. Zhong, J. Ding, X. Wang, L. Chai, T. T. Li, K. Su, Y. Hu, J. Qian and S. Huang, *Inorg. Chem.*, 2020, **59**, 2701-2710.
9. D. Han, K. Huang, X. Li, M. Peng, L. Jing, B. Yu, Z. Chen and D. Qin, *RSC Advances*, 2019, **9**, 33890-33897.
10. W. Zhang, Y. Wang, H. Zheng, R. Li, Y. Tang, B. Li, C. Zhu, L. You, M. R. Gao, Z. Liu, S. H. Yu and K. Zhou, *ACS Nano*, 2020, **14**, 1971-1981.
11. J. T. Yuan, J. J. Hou, X. L. Liu, Y. R. Feng and X. M. Zhang, *Dalton Trans*,

2020, **49**, 750-756.

12. K. Nath, K. Bhunia, D. Pradhan and K. Biradha, *Nanoscale Advances*, 2019, **1**, 2293-2302.

13. X. Ma, C. Chang, Y. Zhang, P. Niu, X. Liu, S. Wang and L. Li, *ACS Sustainable Chemistry & Engineering*, 2020, **8**, 8318-8326.

14. X. Song, C. Peng and H. Fei, *ACS Appl. Energy Mater.*, 2018, **1**, 2446-2451.

15. J. Jiang, L. Huang, X. Liu and L. Ai, *ACS Appl Mater Interfaces*, 2017, **9**, 7193-7201.

16. T. Zhao, J. Gao, J. Wu, P. He, Y. Li and J. Yao, *Energy Technology*, 2019, **7**, 1800969.

17. J. W. Tian, Y. P. Wu, Y. S. Li, J. H. Wei, J. W. Yi, S. Li, J. Zhao and D. S. Li, *Inorg. Chem.*, 2019, **58**, 5837-5843.

18. X. Wang, H. Zhang, Z. Yang, C. Zhang and S. Liu, *Ultrason. Sonochem.*, 2019, **59**, 104714.

19. X. Liu, Y. Liu and L.-Z. Fan, *J. Mater. Chem. A*, 2017, **5**, 15310-15314.

20. M. Yang, W. Zhu, R. Zhao, H. Wang, T.-N. Ye, Y. Liu and D. Yan, *J. Solid State Chem.*, 2020, **288**, 121456.